Physics of the Earth and Planetary Interiors, 53 (1989) 287–297
Elsevier Science Publishers B.V., Amsterdam – Printed in The Netherlands

Calculations of voltages for magnetotelluric modelling of a region with near-surface inhomogeneities

Helena E. Poll and J.T. Weaver

Department of Physics and Astronomy, University of Victoria, Victoria, B.C., V8W 2Y2 (Canada)

Alan G. Jones

Geological Survey of Canada, 1 Observatory Crescent, Ottawa, Ont., K1A 0Y3 (Canada)

(Received December 30, 1986; revision accepted August 20, 1987)

Poll, H.E., Weaver, J.T. and Jones, A.G., 1989. Calculations of voltages for magnetotelluric modelling of a region with near-surface inhomogeneities. Phys. Earth Planet. Inter., 53: 287–297.

In the magnetotelluric method, measurements of the components of the horizontal electric field are obtained by recording the voltage between grounded electrodes and dividing by their separation distances. This procedure gives the true value of the electric field only if it is uniform between the electrodes. In regions of near-surface inhomogeneity this condition is not fulfilled, and in extreme cases each electrode may be in contact with surface material of different resistivity. It is therefore suggested that voltages, rather than electric fields, should be computed in the two-dimensional modelling of such regions in the *B*-polarization mode, and that magnetotelluric impedance calculations for comparison with real data should be based on voltages. A method for modifying an existing finite difference program is described, and sample calculations of voltage differences in the control model of Weaver, LeQuang and Fischer are checked against the exact analytic results that can be obtained. Finally, real data obtained over the Gloucester Fault in Canada are compared with results given by finite difference modelling based both on voltage calculations and on the more conventional electric field calculations.

1. Introduction

In applications of the magnetotelluric method a horizontal component of the electric field is measured by recording the voltage between two earthed electrodes and dividing by their separation distance. In the schematic diagram Fig. 1a the electric field in the y-direction would be given by

$$E_y = \mathscr{V}_{21}/d \tag{1}$$

where $\mathscr{V}_{21}$ is the recorded voltage between electrodes 2 and 1. The electric field measured in this manner is then arbitrarily assigned to a particular point in the range covered by the electrode pair. Typically it is chosen to be at one of the electrode positions although the point midway between the electrodes would seem to be preferable (see also Section 3 and Table I).

Actually the voltage between the two electrodes is correctly defined by the line integral

$$\mathscr{V}_{21} = \int_1^2 \mathbf{E} \cdot \mathrm{d}\mathbf{s} = \int_{y_1}^{y_2} E_y \, \mathrm{d}y \tag{2}$$

which agrees with eqn. (1) only if E_y is constant between the electrodes. (Note that in general the line integral (2) is path dependent, but for the application considered in this paper the value of $\mathscr{V}_{21}$ is always independent of the path of integration.) In regions with near-surface inhomogeneities, such as shown in Fig. 1b, eqn. (1) will give some average value for E_y, while in the extreme case shown in Fig. 1c, where the electrodes are

Geological Survey of Canada Publication 42486.

0031-9201/89/$03.50

TABLE I

Comparison of the true electric field in units of mV km^{-1} nT^{-1} with the analytic and numerical voltage electric fields in the y-direction. The voltage fields were assigned to a point midway between the two points which provided the voltage used in each calculation

y (km)	True analytic		Voltage divided by separation distance			
			Analytic		Numerical	
	Real	Imaginary	Real	Imaginary	Real	Imaginary
−35.000	−0.3122	−0.2879				
−32.000	−0.3142	−0.2873	−0.3143	−0.2873	−0.3143	−0.2884
−29.000	−0.3168	−0.2869				
−26.000	−0.3204	−0.2870	−0.3206	−0.2871	−0.3206	−0.2883
−23.000	−0.3252	−0.2880				
−20.000	−0.3317	−0.2906	−0.3321	−0.2911	−0.3321	−0.2922
−17.000	−0.3406	−0.2962				
−14.500	−0.3507	−0.3055	−0.3512	−0.3070	−0.3510	−0.3080
−12.000	−0.3641	−0.3244				
−11.750	−0.3657	−0.3273	−0.2308	−0.2191	−0.2304	−0.2189
−10.000	−0.3786	−0.3658				
−10.000	−0.0378	−0.0365				
−8.500	−0.0495	−0.0712				
−6.750	−0.0608	−0.0866	−0.0604	−0.0853	−0.0601	−0.0877
−5.000	−0.0696	−0.0940				
−2.500	−0.0783	−0.0982	−0.0777	−0.0977	−0.0772	−0.0990
0.000	−0.0834	−0.0990				
2.500	−0.0854	−0.0982	−0.0849	−0.0980	−0.0843	−0.0992
5.000	−0.0846	−0.0961				
6.750	−0.0825	−0.0933	−0.0823	−0.0929	−0.0817	−0.0942
8.500	−0.0789	−0.0879				
10.000	−0.0745	−0.0752				
10.000	−0.1491	−0.1505				
11.750	−0.1440	−0.1368	−0.1164	−0.1163	−0.1156	−0.1175
12.000	−0.1434	−0.1358				
14.500	−0.1385	−0.1304	−0.1387	−0.1309	−0.1380	−0.1315
17.000	−0.1352	−0.1283				
20.000	−0.1326	−0.1275	−0.1327	−0.1276	−0.1321	−0.1286
23.000	−0.1309	−0.1275				
26.000	−0.1300	−0.1278	−0.1300	−0.1278	−0.1294	−0.1288
29.000	−0.1294	−0.1281				
32.000	−0.1291	−0.1284	−0.1291	−0.1284	−0.1285	−0.1294
35.000	−0.1289	−0.1286				

Model parameters: $a = 10.0$ km; $d = 50.0$ km; $T = 300.0$ s; $\sigma_1 = 0.10$ S m^{-1}; $\sigma_2 = 1.00$ S m^{-1}; $\sigma_3 = 0.50$ S m^{-1}.

embedded in surface materials of different conductivities σ_1 and σ_2, E_y is actually discontinuous across the boundary between the two regions and eqn. (1) could become quite inaccurate, as noted previously by Fischer et al. (1983). Thus, in general, the electric fields computed by numerical modelling programs are not the same values as those measured by voltages. In order to compare model with experiment on an equal basis it is therefore proposed that voltage divided by electrode separation be used as the 'electric field' in model calculations when comparisons with real data are made. For two-dimensional calculations, only the B-polarization formulae will require mod-

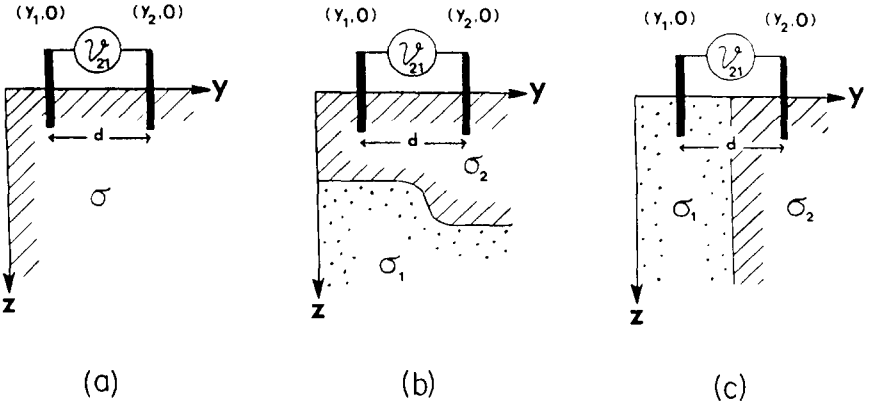

Fig. 1. Schematic diagram of the measurement of the voltage between two electrodes earthed (a) in a homogeneous region, (b) in a region with a near-surface inhomogeneity, and (c) across a fault.

ification; by definition the electric field E_x in the E-polarization mode is constant along any line in the x-direction.

It is the purpose of this paper to show how an existing two-dimensional finite difference program can be amended so that voltages between nodes rather than electric fields are calculated at each node of the numerical grid in the B-polarization model. In order to investigate how 'electric field' values obtained from voltages differ from those calculated directly we have compared the two sets of results with the synthetic control model examined previously by Weaver et al. (1985). Since an analytic solution is available for this model, we are also able to check the accuracy of the voltage values given by the modified program. Finally, we compare model calculations using voltages with field results obtained over the Gloucester Fault in Ontario, Canada, a structure known to resemble the configuration shown in Fig. 1c.

2. Finite difference expressions for voltage

Since we wish to use $\mathscr{V}_{21}$ rather than the electric field we need to calculate the voltage between grid points on the surface of a two-dimensional numerical model. Consider a node, $y = y_m (m = 2, \ldots, M-1)$ as shown in Fig. 2. The notation we use is the same as in Brewitt-Taylor and Weaver (1976) (also Weaver et al., 1985) except that the second subscripts on the parameters (indicating the grid co-ordinate number in the z-direction) are omitted since we are working only on the surface $z = 0$. The y and z components of the electric field are denoted by $V(y, z)$ and $W(y, z)$ respectively, with time dependence $\exp(i\omega t)$ understood, and at the surface nodes we write $V(y_m \pm 0,0) = V_m^{\pm}$, $W(y_m \pm 0,0) = W_m$, the latter being uniquely defined by continuity of the tangential electric field. With μ_0 denoting vacuum permeability (assumed throughout the model) we also define

$$\rho_{m\pm1/2} = \frac{1}{\omega\mu_0\sigma_{m\pm1/2}}$$
$$\rho_m = \frac{h_{m-1}\rho_{m-1/2} + h_m\rho_{m+1/2}}{h_{m-1} + h_m} \tag{3}$$

On the boundary $y = y_m$ continuity of normal current density requires

$$V_m^-/\rho_{m-1/2} = V_m^+/\rho_{m+1/2} \tag{4}$$

and continuity of $\partial W/\partial z$ (following from the continuity of W) together with the fact that div $\mathbf{E} = 0$ in each cell, gives

$$\left(\frac{\partial V}{\partial y}\right)_m^- = -\left(\frac{\partial W}{\partial z}\right)_m^- = -\left(\frac{\partial W}{\partial z}\right)_m^+ = \left(\frac{\partial V}{\partial y}\right)_m^+ \tag{5}$$

Since $\mathbf{E}$ satisfies $\nabla^2\mathbf{E} = i\omega\mu_0\sigma\mathbf{E}$ in a cell of conductivity σ, we have

$$\left(\frac{\partial^2 V}{\partial y^2}\right)_m^+ = \frac{iV_m^+}{\overline{\rho_{m+1/2}}} - \left(\frac{\partial^2 V}{\partial z^2}\right)_m^+$$
$$= i\left(\frac{\rho_{m-1/2} - \rho_{m+1/2}}{\rho_{m-1/2}^2}\right)V_m^-$$
$$+ \frac{\rho_{m+1/2}}{\rho_{m-1/2}}\left(\frac{\partial^2 V}{\partial y^2}\right)_m^- \qquad (6)$$

the last step following by successive application of (4).

The results (4) and (6) constitute boundary conditions on the (discontinuous) fields V and $\partial^2 V/\partial y^2$ at a surface node on the vertical boundary between two cells of different conductivity. Boundary condition (5) shows that $\partial V/\partial y$ is continuous at such a node.

The finite difference program of Brewitt-Taylor and Weaver (1976) is based on central difference formulae which are obtained by expanding the field up to second-order terms, and it is therefore desirable to calculate voltages to the same accuracy. A Taylor expansion of V on either side of the node y_m yields

$$V_{m+1}^- = V_m^+ + h_m\left(\frac{\partial V}{\partial y}\right)_m^+ + \frac{h_m^2}{2}\left(\frac{\partial^2 V}{\partial y^2}\right)_m^+ \qquad (7)$$

$$V_{m-1}^+ = V_m^- - h_{m-1}\left(\frac{\partial V}{\partial y}\right)_m^- + \frac{h_{m-1}^2}{2}\left(\frac{\partial^2 V}{\partial y^2}\right)_m^- \qquad (8)$$

Adding eqn. (7) multiplied by h_{m-1} to eqn. (8) multiplied by h_m and using boundary conditions (5) and (6) we obtain, with the aid of (3)

$$\left(\frac{\partial^2 V}{\partial y^2}\right)_m^+ = \frac{2\rho_{m+1/2}}{\rho_m(h_m + h_{m-1})}\left(\frac{V_{m+1}^- - V_m^+}{h_m} - \frac{V_m^- - V_{m-1}^+}{h_{m-1}}\right)$$
$$+ \frac{ih_{m-1}V_m^-}{\rho_m(h_m + h_{m-1})}\left(1 - \frac{\rho_{m+1/2}}{\rho_{m-1/2}}\right) \qquad (9)$$

This is a generalization of the finite difference formula for $\partial^2 V/\partial y^2$ at a conductivity boundary. If $\rho_{m+1/2} = \rho_{m-1/2} = \rho_m$, it reduces to the familiar central difference representation of the second derivative. To find an expression for voltage between the nodes y_{m+1} and y_m we now represent V in $y_m < y < y_{m+1}$ by the Taylor expansion

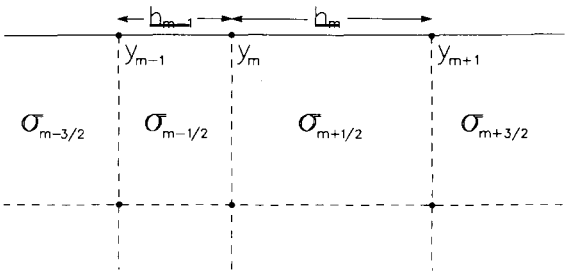

Fig. 2. A surface node (m) in the numerical grid for finite difference calculations.

$$V(y) = V_m^+ + (y - y_m)\left(\frac{\partial V}{\partial y}\right)_m^+ + \frac{(y - y_m)^2}{2}\left(\frac{\partial^2 V}{\partial y^2}\right)_m^+$$

and integrate over y from y_m to y_{m+1} according to (2), to obtain

$$\mathscr{V}_{m+1,m} = \tfrac{1}{2}h_m(V_m^+ + V_{m+1}^-) - \frac{h_m^3}{12}\left(\frac{\partial^2 V}{\partial y^2}\right)_m^+ \qquad (10)$$

where (7) has been used to eliminate $(\partial V/\partial y)_m^+$ from the final result.

Finally, the expression (9) can be substituted for $(\partial^2 V/\partial y^2)_m^+$ in (10), and to avoid two separate calculations of the electric field (one for the right-hand side values V_m^+ and one for the left-hand side values V_m^-) everything can be expressed in terms of right-hand side values through boundary condition (4). After some lengthy algebraic rearrangement we arrive at the final result

$$\mathscr{V}_{m+1,m} = \frac{h_m^2\rho_{m+1/2}}{6\rho_m(h_m + h_{m-1})}\left\{\left[4 + \left(\frac{3h_{m-1}}{h_m} + \frac{h_m}{h_{m-1}}\right)\frac{\rho_{m-1/2}}{\rho_{m+1/2}} + \frac{ih_mh_{m-1}}{2\rho_{m+1/2}}\right.\right.$$
$$\left.\times\left(1 - \frac{\rho_{m-1/2}}{\rho_{m+1/2}}\right)\right]V_m^+ + \left[\frac{2\rho_{m+1/2}}{\rho_{m+3/2}}\right.$$
$$\left.\left. + \frac{3h_{m-1}}{h_m}\frac{\rho_{m-1/2}}{\rho_{m+3/2}}\right]V_{m+1}^+ - \frac{h_mV_{m-1}^+}{h_{m-1}}\right\} \qquad (11)$$

($m = 2, \ldots, M-1$), which is the desired finite difference formula giving the voltage between two adjacent nodes on the surface of the numerical grid. A similar expression could be derived in terms of left-hand side values if required.

It is worth noting that if the near-surface inhomogeneities do not actually reach the surface itself (as in Fig. 1b, for example), so that $\rho_{m-1/2} = \rho_{m+1/2} = \rho_{m+3/2} = \rho_m$, then (11) reduces to the much simplified form

$$\mathscr{V}_{m+1,m} = \frac{h_m}{6}\{(3 + r_m)V_m - r_m s_m V_{m-1} + (3 - s_m)V_{m+1}\} \quad (12)$$

where $r_m = h_m/h_{m-1}$ and $s_m = r_m/(1 + r_m)$.

3. Analytic control model

In order to investigate the accuracy of our finite difference calculations of voltages we modified an existing B-polarization analytic solution obtained by Weaver et al. (1985) for the control model shown in Fig. 3. It is shown in the Appendix how their solution can be integrated to give an analytic expression for the voltage $\mathscr{V}(y; 0)$ between any point y on the surface and the origin. The voltage between the nodes y_{m+1} and y_m can then be calculated from the formula

$$\mathscr{V}_{m+1,m} = \mathscr{V}(y_{m+1}; 0) - \mathscr{V}(y_m; 0)$$

The voltage solutions were programmed for numerical calculation and the resulting 'electric field' values were obtained for the control model shown. The model parameters used were $T = 2\pi/\omega = 300$ s, $a = 10$ km, $d = 50$ km, $\sigma_1 = 0.1$ S m^{-1}, $\sigma_2 = 1.0$ S m^{-1}, $\sigma_3 = 0.5$ S m^{-1}.

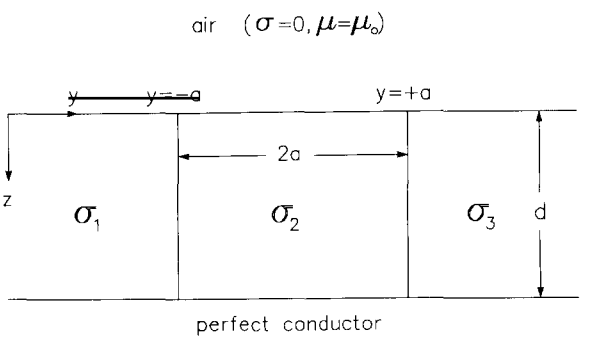

Fig. 3. The control model used in the comparison of true electric fields and those given by voltage divided by separation distance.

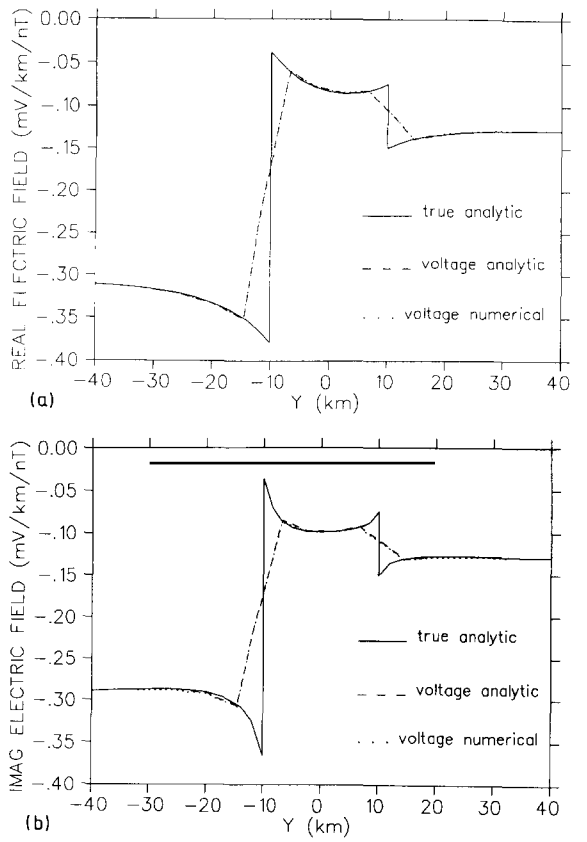

Fig. 4. Variation of the (a) real and (b) imaginary parts of the horizontal component V of the electric field across the surface of the control model as given by direct analytic calculation (solid line), by analytic computation of voltage values (broken line), and by numerical computation of voltage values (dotted line). Note that the accuracy of the numerical values is such that the two voltage curves are barely distinguishable from each other.

In Fig. 4 and Table I the analytic values for the true electric field and the corresponding analytic and numerical values obtained from voltage calculations are compared. The excellent agreement between the two fields given by voltage calculations illustrates the accuracy of our finite difference expressions for voltages. However, it is clear that the voltage 'electric field' is only an approximation to the true electric field. Away

from conductivity boundaries the two methods of calculation give the same results but on and near the boundaries there is considerable error in estimating electric fields by voltage calculations.

In the above comparison the 'electric field' was assigned to the point midway between the two electrodes measuring the voltage. It can be seen from Table I that this results in a more accurate representation of the field than if the electric field value were assigned to one of the two electrode positions. Unfortunately, this latter course of action is followed in most experimental studies.

4. Field results from the Gloucester Fault

We now turn to actual field measurements where a profile of electrodes is known to traverse a fault: the Gloucester Fault in Ontario, Canada. The field data shown in Fig. 5 illustrate dramatically the large attenuation of the electric fields obtained from voltage measurements between sites only 50 m apart. Obviously, this is a case where eqn. (1) will not be valid for the electrode pairs straddling the fault or those nearby. The profile of perpendicular electrode pairs is shown in Fig. 6; the separation of the electrodes in each direction is 50 m (except between electrodes 7 and 8, where it is 40 m). The electric fields in each direction are given by the measured voltage divided by 50 m, and are assigned to the common electrode (nos. 1–8) in each perpendicular pair. Magnetic recordings were taken by EDA magnetometers at points 1 and 8; in addition, PHOENIX MT measure-

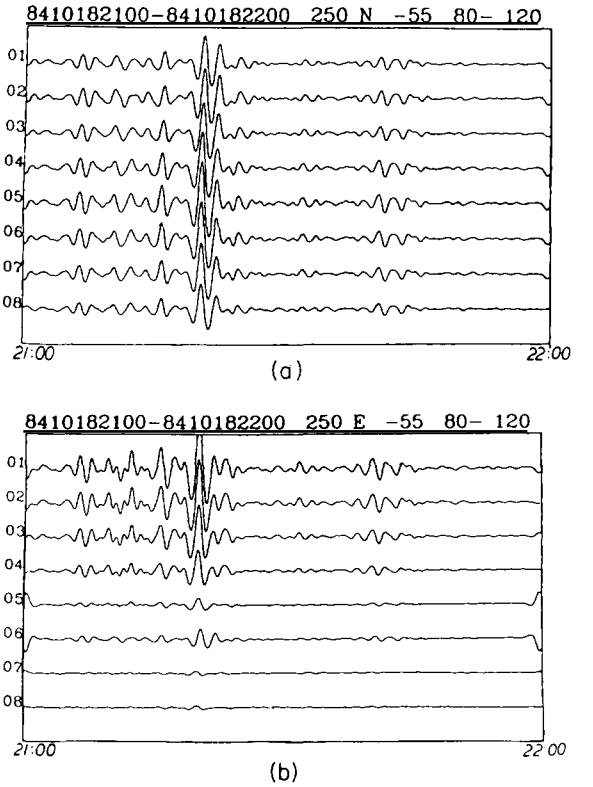

Fig. 5. Electric field data from the Gloucester Fault, Ontario, Canada: (a) parallel to the fault, (b) perpendicular to the fault.

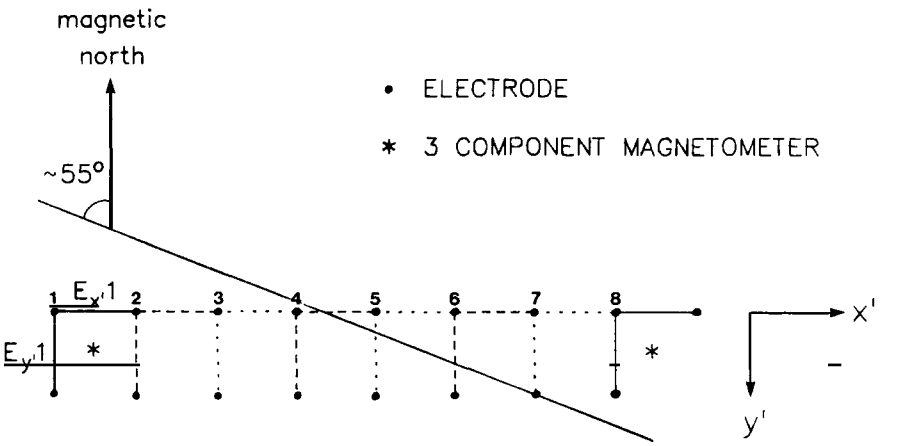

Fig. 6. Orientation and position of the electrode profile across the Gloucester Fault.

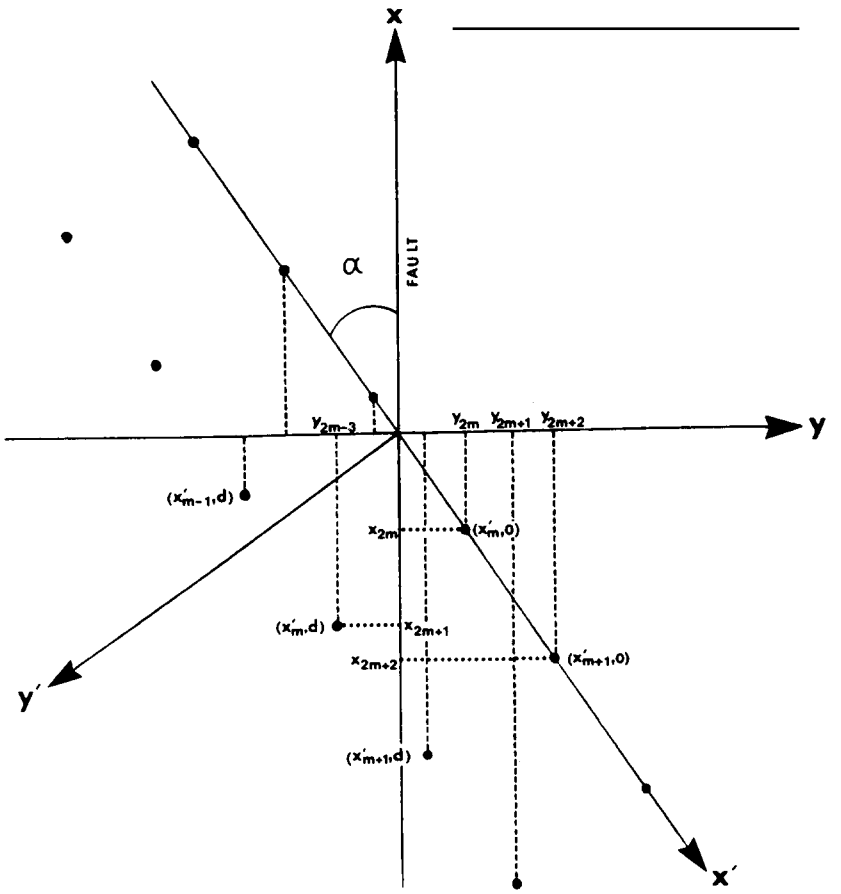

Fig. 7. Notation used to transform the measured orthogonal horizontal components of electric field ($\tilde{U}'$, $\tilde{V}'$) into components ($\tilde{U}$, $\tilde{V}$) parallel and perpendicular to the strike.

ments were made at the centre of the squares whose sides are formed by the perpendicular electrode pairs meeting at positions 1 and 8. Since the fields we want to study are the electric fields perpendicular and parallel to the strike and not those along the (x', y') axes defined by the electrode pairs, we must first perform a transformation.

As shown in Fig. 7, the electrode stations are labelled in ascending order along the x'-axis in the direction of increasing x'. Thus the mth station has co-ordinates (x'_m, 0) in the primed co-ordinate system and the transverse station at the mth point has co-ordinates (x'_m, d) where $d \equiv x'_{m+1} - x'_m$ is the separation of the electrodes. Now the mth station, (x'_m, 0) has co-ordinates (x_{2m}, y_{2m}) in the unprimed co-ordinate system and the corresponding transverse station at (x'_m, d) has co-ordinates (x_{2m+1}, y_{2m-3}). Note that this notation holds only for strike angles $\alpha < \pi/4$. On the Gloucester Fault the electrodes were aligned with $\alpha = 35°$. The equations of transformation are clearly

$$\begin{aligned} x' &= -x \cos\alpha + y \sin\alpha \\ x &= -x' \cos\alpha - y' \sin\alpha \\ y' &= -x \sin\alpha - y \cos\alpha \\ y &= x' \sin\alpha - y' \cos\alpha \end{aligned} \tag{13}$$

Likewise, the horizontal electric field components on the surface $z = 0$ satisfy the same transforma-

tion eqns. (13) which, for a B-polarization field (i.e., $U(y) = 0$), reduce to

$$U'(x', y') = V(y) \sin \alpha$$
$$U(y) = 0$$
$$V'(x', y') = -V(y) \cos \alpha$$
$$V(y) = U'(x', y') \sin \alpha - V'(x', y') \cos \alpha \tag{14}$$

Here U', V' are the horizontal components of the electric field in the electrode (primed) co-ordinate system. The components U'_m, V'_m at station m are measured in the field as

$$\tilde{U}'_m = \mathscr{V}(x'_{m+1}, 0; x'_m, 0)/d$$
$$\tilde{V}'_m = \mathscr{V}(x'_m, d; x'_m, 0)/d$$

where $\mathscr{V}(x'_1, y'_1; x'_2, y'_2)$ is the voltage measured along the straight line between (x'_1, y'_1) and (x'_2, y'_2), and where the tilde denotes an electric field given by voltage divided by separation distance. By eqns. (1) and (2) we obtain

$$\tilde{U}'_m = \frac{1}{d}\int_{x'_m}^{x'_{m+1}} U'(x', 0)\, dx'$$
$$\tilde{V}'_m = \frac{1}{d}\int_0^d V'(x', y')\, dy' \tag{15}$$

We can transform the integrals (15) into the unprimed co-ordinate system by using eqns. (13) and (14), which give

$$\tilde{U}'_m = \frac{1}{d}\int_{y_{2m}}^{y_{2m+2}} V(y)\, dy$$
$$\tilde{V}'_m = \frac{1}{d}\int_{y_{2m}}^{y_{2m-3}} V(y)\, dy \tag{16}$$

Now $y_{2m+2} = y_{2m} + d\sin\alpha$ and $y_{2m-3} = y_{2m} - d\cos\alpha$ and by analogy with (13), we have

$$\tilde{U}_m = -\tilde{U}'_m \cos\alpha - \tilde{V}'_m \sin\alpha$$
$$\tilde{V}_m = \tilde{U}'_m \sin\alpha - \tilde{V}'_m \cos\alpha$$

which, combined with (16), give

$$\tilde{U}_m = \frac{\sin\alpha}{d}\int_{y_{2m}-d\cos\alpha}^{y_{2m}} V(y)\, dy - \frac{\cos\alpha}{d}\int_{y_{2m}}^{y_{2m}+d\sin\alpha} V(y)\, dy$$
$$\tilde{V}_m = \frac{\cos\alpha}{d}\int_{y_{2m}-d\cos\alpha}^{y_{2m}} V(y)\, dy + \frac{\sin\alpha}{d}\int_{y_{2m}}^{y_{2m}+d\sin\alpha} V(y)\, dy \tag{17}$$

It is interesting to note than even though we started with a 2-dimensional B-polarization model in which $U = 0$, the use of voltages to calculate electric fields has introduced a spurious electric field $\tilde{U}$. This would disappear, of course, if the electrode profile were aligned perpendicularly to the fault ($\alpha = \pi/2$).

The geology of the Gloucester Fault region is shown in Fig. 8 (Telford et al., 1977) and an idealized two-dimensional model for numerical modelling is shown in Fig. 9. This model was used in the finite difference program to obtain both the true electric field and the 'electric field' from voltages for a period of 100 s. For a simple comparison of the observed electric fields in Fig. 5 with these results, the field variations at each station were filtered with a bandwidth 80–120 s

TABLE II

Comparison of the magnitudes of the electric field variations in mV km^{-1} given by the full range (trough to peak) amplitudes of their sine wave representations

Station	Experimental $\lvert E_\perp \rvert$	True $\lvert E_\perp \rvert$	Voltage divided by separation distance $\lvert E_\perp \rvert$	Voltage divided by separation distance $\lvert E_\parallel \rvert$
1	68.7	68.7	68.7	0.31
2	58.2	69.3	69.1	0.31
3	44.4	69.9	69.8	0.38
4	29.0	70.8	52.2	25.7
5	9.76	1.82	22.1	14.1
6 [a]	15.1	2.19	2.05	0.17
7	3.48	2.36	2.28	0.08
8	3.10	2.43	2.27	0.14

[a] 15–20 s delay believed to be instrument problem.

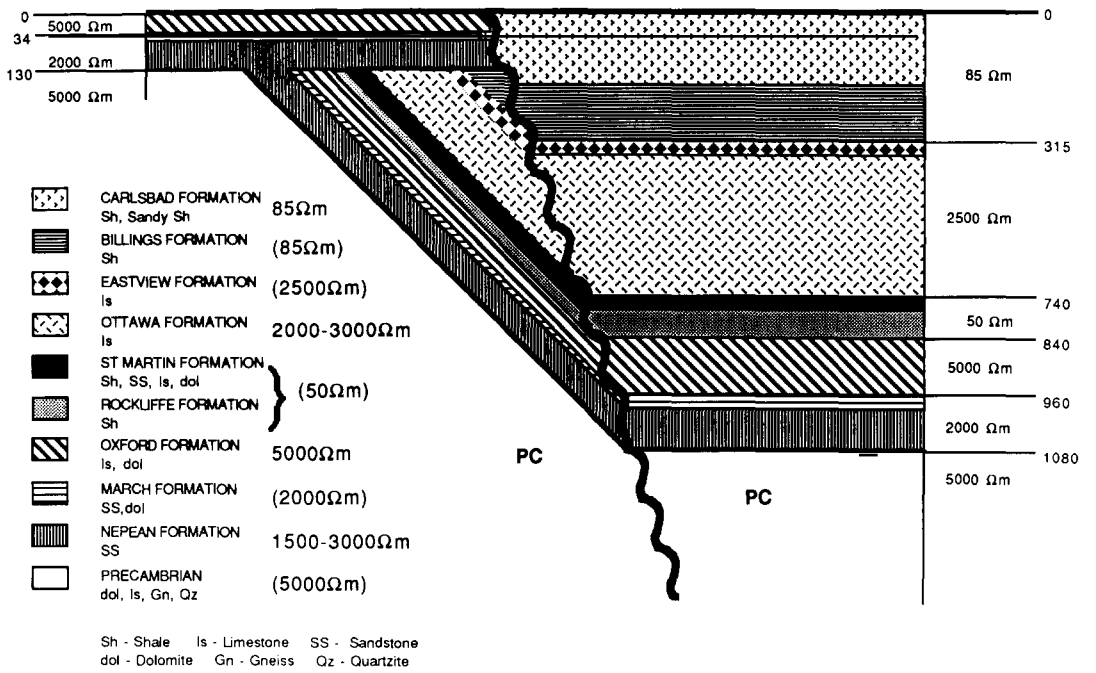

Fig. 8. Geology and electrical conductivities of the Gloucester Fault region. Conductivities are from Telford et al. (1977), except for those in brackets which are assumed values based on the conductivities of similar rock types in the area. Depths are in metres.

(−3 dB points), and were then assumed to be sinusoidal in time (period 100 s) with the peak value occurring at time 21 : 20 : 10 and the adjacent troughs at 21 : 19 : 15 and 21 : 21 : 00. In Table II, the full range amplitudes of the electric field between trough and peak (i.e., twice the amplitude of the sine wave) are listed for each station in units of mV km^{-1} and are compared with the corresponding values given by our true electric field and voltage calculations. These latter values were normalized by the measured values at Station 1 (as far removed from the fault as possible) before tabulation. Also shown are the values of the component of electric field (similarly normalized) parallel to the fault given by the voltage calculation according to the first of eqns. (17). These are not real fields; they are manifestations of the inaccuracies in the method of measuring the electric field, and, as expected, are very small except for the electrode pairs that straddle the fault.

It can be seen from Table II that neither the calculated true electric field nor the voltage computation are in close agreement with the measured field values in the region of the fault. However, the results given by voltage divided by separation distance clearly represent a better approximation to the observed behaviour of the measured electric field than the computed values of the true electric field, particularly at Station 4. The latter actually increases slightly between Stations 3 and 4 whereas the amplitude of the observed field shows a steep decline from Stations 3 to 5. This decline is much more faithfully reproduced by the voltage calculations. The spurious electric field parallel to the fault shown in column 5 of Table II is surprisingly large at Stations 4 and 5 (49 and 64% respectively of the corresponding fields perpendicular to the fault), thereby revealing another source of error inherent in field measurements involving the magnetotelluric method. It is to be expected that an *E*-polarization field will contribute in a similar manner to the field measured by voltages perpendicular to the fault, but no attempt has been made in this study to estimate the contribution from an *E*-polarization field to the total ampli-

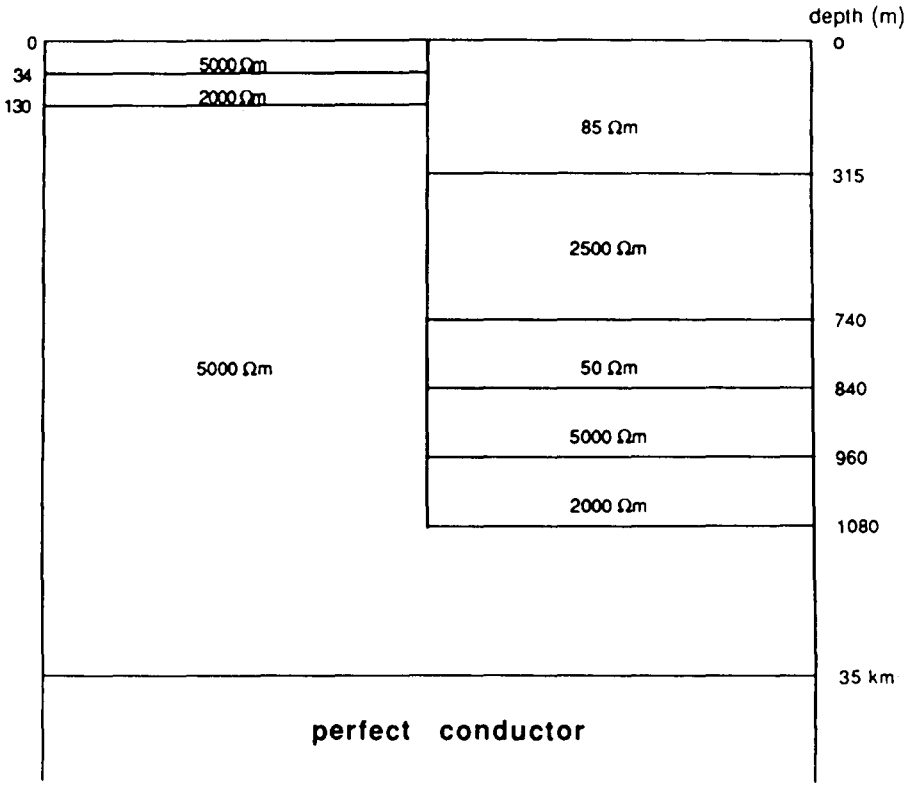

Fig. 9. Idealized model of the Gloucester Fault used in the numerical calculations.

tude of the perpendicular electric field in the neighbourhood of the fault.

5. Conclusions

In the magnetotelluric method comparisons are usually made between modelled and observed apparent resistivities and phases, but these parameters are, of course, affected by the electric field values. The main purpose of this paper is to draw attention to possible sources of error in the interpretation of measured apparent resistivity and phase values when comparing them with model calculations in regions where the electrode profile crosses a geological fault. In particular, it is recommended that model calculations use voltage divided by separation distance to compute the electric fields for comparison with real data.

Acknowledgements

J.T.W. gratefully acknowledges financial support in the form of an operating grant from the Natural Sciences and Engineering Research Council of Canada.

Appendix

For the conductivity model shown in Fig. 3, with the inducing magnetic field along the x-axis

(B-polarization), Weaver et al. (1985) obtained the solution for the y-component of the electric field V_j (where $j = 1, 2, 3$ for the three regions of conductivity σ_1, σ_2, σ_3) in the form

$$\frac{V_j}{B_0} = \frac{-\omega}{\alpha_j}\left\{\frac{\sqrt{i}\,\sinh\left[(d-z)\alpha_j\sqrt{i}\right]}{\cosh\left(d\alpha_j\sqrt{i}\right)} - \frac{1}{\alpha_j}\sum_{m=0}^{\infty} k_m F_m^{(j)}(y)\cos(k_m z)\right\} \qquad \text{(A1)}$$

where $\alpha_j^2 = \omega\mu_0\sigma_j$ and $k_m = (2m+1)\pi/2d$. The Fourier series coefficients are given as

$$\begin{aligned} F_m^{(j)}(y) &= P_m^{(j)} \exp\left[(a - |y|)\gamma_m^{(j)}\right] \quad (j = 1, 3) \\ F_m^{(2)}(y) &= L_m^{(1)} \exp\left[-(y+a)\gamma_m^{(2)}\right] \\ &\quad + L_m^{(3)} \exp\left[(y-a)\gamma_m^{(2)}\right] \end{aligned} \qquad \text{(A2)}$$

where for $j = 1, 3$

$$P_m^{(j)} = \frac{\beta_m^{(j)}}{D_m}\left\{2\bar{K}_m^{(j)} \exp\left(-2a\gamma_m^{(2)}\right) - K_m^{(j)}\left[1 + \bar{\beta}_m^{(j)} + \left(1 - \bar{\beta}_m^{(j)}\right)\exp\left(-4a\gamma_m^{(2)}\right)\right]\right\}$$

$$L_m^{(j)} = \frac{1}{D_m}\left[\left(1 + \bar{\beta}_m^{(j)}\right)K_m^{(j)} - \left(1 - \beta_m^{(j)}\right)\bar{K}_m^{(j)} \exp\left(-2a\gamma_m^{(2)}\right)\right]$$

$$K_m^{(j)} = \frac{2ik_m\left(\alpha_2^2 - \alpha_j^2\right)}{d\left(\gamma_m^{(2)}\gamma_m^{(j)}\right)^2} \qquad \bar{K}_m^{(j)} = \frac{K_m^{(1)}K_m^{(3)}}{K_m^{(j)}}$$

$$\beta_m^{(j)} = \frac{\gamma_m^{(2)}/\sigma_2}{\gamma_m^{(j)}/\sigma_j} \qquad \bar{\beta}_m^{(j)} = \frac{\beta_m^{(1)}\beta_m^{(3)}}{\beta_m^{(j)}}$$

and where we have defined

$$D_m = \left(1 + \beta_m^{(1)}\right)\left(1 + \beta_m^{(3)}\right) - \left(1 - \beta_m^{(1)}\right)\left(1 - \beta_m^{(3)}\right)\exp\left(-4a\gamma_m^{(2)}\right)$$

$$\gamma_m^{(j)} = \sqrt{k_m^2 + i\alpha_j^2}$$

Note that $F_m^{(2)}(y)$ as given by (A2) is slightly different from (but equivalent to) the form quoted by Weaver et al. (1985). As a matter of fact (A2) was the expression they actually used in their program, and it is not only algebraically simpler than the one quoted in the previous paper but also more convenient for programming. Let $\mathscr{V}(y_1; y_2)$ be the voltage between points $(y_1, 0)$ and $(y_2, 0)$ on the surface. Then according to (2)

$$\mathscr{V}(y; 0) = \begin{cases} \mathscr{V}(-a; 0) + \int_{-a}^{y} V_1\,\mathrm{d}y & (y < -a) \\ \int_{0}^{y} V_2\,\mathrm{d}y & (-a \leqslant y \leqslant a) \\ \mathscr{V}(a; 0) + \int_{a}^{y} V_3\,\mathrm{d}y & (y > a) \end{cases}$$

Integrating the expressions (A1) and setting $z = 0$ we obtain

$$\mathscr{V}(y; 0) = \mathscr{V}(\mp a; 0) - \omega(y \pm a)\sqrt{i}\,\tanh\left(d\alpha_j\sqrt{i}\right) \pm \frac{\omega}{\alpha_j^2}\sum_{m=0}^{\infty}\frac{k_m}{\gamma_m^{(j)}}\left[F_m^{(j)}(y) - P_m^{(j)}\right]$$

for $|y| > a$, with the upper sign and $j = 1$ applying for $y < -a$ and the lower sign and $j = 3$ for $y > a$. In $-a \leqslant y \leqslant a$ we have

$$\mathscr{V}(y; 0) = -\omega y\sqrt{i}\,\tanh\left(d\alpha_2\sqrt{i}\right) + \frac{\omega}{\alpha_2^2}\sum_{m=0}^{\infty}\frac{k_m}{\gamma_m^{(2)}}\left\{L_m^{(3)} \exp\left[(y-a)\gamma_m^{(2)}\right] - L_m^{(1)} \exp\left[-(y+a)\gamma_m^{(2)}\right]\right\}$$

References

Brewitt-Taylor, C.R. and Weaver, J.T., 1976. On the finite difference solution of two-dimensional induction problems. Geophys. J. R. Astron. Soc., 47: 375–396.

Fischer, G., LeQuang, B.V. and Müller, I., 1983. VLF ground surveys, a powerful tool for the study of shallow two-dimensional structures. Geophys. Prospect., 31: 977–991.

Telford, W.N., King, W.F. and Becker, A., 1977. VLF mapping of geological structure. Geol. Surv. Can., Paper 76-25.

Weaver, J.T., LeQuang, B.V. and Fischer, G., 1985. A comparison of analytical and numerical results for a two-dimensional control model in electromagnetic induction – I. B-polarization calculations. Geophys. J. R. Astron. Soc., 82: 263–278.